



ELSEVIER

Coastal Engineering 32 (1997) 91–117

**COASTAL
ENGINEERING**

Time-dependent equations for wave propagation on rapidly varying topography

Kyung Doug Suh^{a,*}, Changhoon Lee^b, Woo Sun Park^b

^a *Department of Civil Engineering, Seoul National University, Seoul 151-742, South Korea*

^b *Coastal Engineering Division, Korea Ocean Research and Development Institute, Ansan P.O. Box 29, Seoul 425-600, South Korea*

Received 22 August 1996; accepted 3 March 1997

Abstract

Two time-dependent equations for wave propagation on rapidly varying topography are developed using different theoretical approaches and are shown to be identical. The developed equations include higher-order bottom effect terms proportional to the square of bottom slope and to the bottom curvature. Without these higher-order terms, the equations developed are reduced to the time-dependent mild-slope equations of Smith and Sprinks and Radder and Dingemans, respectively. For a monochromatic wave, the equation reduces to the extended refraction–diffraction equation of Massel or the modified mild-slope equation of Chamberlain and Porter, which in turn, without the higher-order terms, reduces to the Berkhoff’s mild-slope equation. For a monochromatic wave, the theory is verified against other theoretical and experimental results related to the waves propagating over a plane slope with different inclination and over a patch of periodic ripples. For random waves, numerical tests are made for the transmission of unidirectional random waves normally incident on a finite ripple patch. © 1997 Elsevier Science B.V.

Keywords: Numerical model; Surface waves; Wave equation; Wave scattering

1. Introduction

The mild-slope equation developed by Berkhoff (1972) has not only been used in its original form of an elliptic equation but also provided the basic governing equation for the development of other wave equations such as the parabolic equation (Radder, 1979)

* Corresponding author. Fax: +82-2-887-0349; e-mail: kdsuh@plaza.snu.ac.kr.

[†] Formerly, Principal Research Engineer, Korea Ocean Research and Development Institute.

and hyperbolic equations (Copeland, 1985), allowing the generation of numerical models which could predict reasonably well the evolution of monochromatic waves due to the combined effect of refraction and diffraction in coastal waters. As an effort towards modeling the propagation of random waves, time-dependent mild-slope equations have also been developed. Smith and Sprinks (1975) developed a hyperbolic time-dependent mild-slope equation using Green's formula and Radder and Dingemans (1985) proposed a canonical form of the time-dependent mild-slope equations based on the Hamiltonian theory of surface waves. Radder and Dingemans' equations consist of two equations for two unknowns of the water surface elevation and the velocity potential at the free surface. Radder and Dingemans showed that their equations could be reduced to the Smith and Sprinks' equation by eliminating the surface elevation. Kubo et al. (1992) also developed another type of time-dependent mild-slope equation using the Taylor series expansion technique for waves with local frequencies different from the carrier frequency. The linear dispersive properties of the time-dependent mild-slope equations were verified by Kirby et al. (1992) and Kubo et al. (1992), who simulated the propagation of wave groups using, respectively, the equation of Radder and Dingemans and the equation of Kubo et al. Recently, on the other hand, Nadaoka et al. (1994) developed a time-dependent nonlinear mild-slope equation which was shown to be the nonlinear extension of the equation of Smith and Sprinks.

In the aforementioned models, the mild-slope assumption $\nabla h/kh \ll 1$ (where $\nabla =$ horizontal gradient operator, $h =$ water depth and $k =$ wavenumber) was made so that the terms of $O((\nabla h)^2)$ and $O(\nabla^2 h)$ were neglected. Recently, by using the Galerkin-eigenfunction method, Massel (1993) developed an extended refraction–diffraction equation which includes these higher-order bottom effect terms as well as the evanescent modes. More recently, Chamberlain and Porter (1995) proposed a modified mild-slope equation which includes the higher-order bottom effect terms as in Massel's equation but not the evanescent modes. Both Massel (1993) and Chamberlain and Porter (1995) demonstrated the applicability of their equations to rapidly varying bottom topography for which Berkhoff's mild-slope equation could fail to produce adequate approximations.

In the present study, using Green's formula method and the Lagrangian formulation, we derive two equivalent time-dependent wave equations for the propagation of water waves on rapidly varying bottom topography. Without the higher-order bottom effect terms, each of the derived equations reduces to the time-dependent mild-slope equations developed by Smith and Sprinks (1975) and Radder and Dingemans (1985), respectively. A reduced form of the derived equation for a monochromatic wave is the same as the modified mild-slope equation developed by Chamberlain and Porter (1995) and the Massel (1993) equation with the evanescent modes neglected.

For the case of a monochromatic wave, first the developed equation is applied to the problem of wave reflection from a plane slope with different inclination, which has been tested by Booij (1983) to examine the accuracy of the mild-slope equation with respect to bottom slope. Second, the equation is applied to the problem of resonant Bragg reflection of monochromatic waves due to singly or doubly periodic ripples to show its capability for rapidly varying topography. Finally, in order to investigate the applicability of the time-dependent wave equation to random waves, numerical tests were made

for the transmission of unidirectional random waves normally incident on a finite ripple patch.

2. Derivation of the wave equations

As mentioned in Section 1, the time-dependent mild-slope equations have been derived using either Green's formula (Smith and Sprinks, 1975) or the Hamiltonian theory of surface waves (Radder and Dingemans, 1985). The latter is equivalent to the Lagrangian formulation of Kirby (1984). Here we adopt the same approach keeping the higher-order bottom effect terms neglected in the previous derivations of the time-dependent mild-slope equations.

2.1. Green's formula method

In the classical linear theory of water waves, the velocity potential $\phi(x, y, z, t)$ is governed by

$$\nabla^2\phi + \phi_{zz} = 0 \quad (-h \leq z \leq 0) \quad (1)$$

$$\phi_z = -\frac{1}{g}\phi_{tt} \quad (z = 0) \quad (2)$$

$$\phi_z = -\nabla h \cdot \nabla\phi \quad (z = -h), \quad (3)$$

where g is the gravitational acceleration and the vertical coordinate z is measured vertically upwards from the still water level. The solution to Eqs. (1)–(3) may be expressed as

$$\phi(x, y, z, t) = f(x, y, z)\tilde{\phi}(x, y, t) + \Sigma\text{nonpropagating modes}, \quad (4)$$

where $f = \cosh k(h+z)/\cosh kh$ is a slowly varying function in the horizontal coordinate (x, y) . The wavenumber $k(x, y)$ must satisfy the dispersion relationship, which relates k to the wave angular frequency ω and the water depth $h(x, y)$ by

$$\omega^2 = gk \tanh kh. \quad (5)$$

In order to extract the propagating component of ϕ , we apply Green's second identity to f and ϕ

$$\int_{-h}^0 (f\phi_{zz} - \phi f_{zz})dz = [f\phi_z - \phi f_z]_{-h}^0. \quad (6)$$

Neglecting the nonpropagating modes and using Eqs. (1)–(4), the integrals are manipulated to finally obtain

$$\tilde{\phi}_{tt} - \nabla \cdot (CC_g \nabla \tilde{\phi}) + (\omega^2 - k^2 CC_g)\tilde{\phi} - g \left(\nabla h \cdot [f \nabla f]_{z=-h} + \int_{-h}^0 f \nabla^2 f dz \right) \tilde{\phi} = 0, \quad (7)$$

where C and C_g are the phase speed and group velocity, respectively. The terms in the last parenthesis of the preceding equation are $O((\nabla h)^2)$ and $O(\nabla^2 h)$ and were neglected

in the equation of Smith and Sprinks (1975). Here, we keep these terms to include the effect of rapid depth variation. Using the following relationships:

$$\nabla f = \left(\frac{\partial f}{\partial h} + \frac{\partial f}{\partial k} \frac{\partial k}{\partial h} \right) \nabla h \quad (8)$$

$$\nabla^2 f = \frac{\partial}{\partial x} \left(\frac{\partial f}{\partial h} \frac{\partial h}{\partial x} + \frac{\partial f}{\partial k} \frac{\partial k}{\partial h} \frac{\partial h}{\partial x} \right) + \frac{\partial}{\partial y} \left(\frac{\partial f}{\partial h} \frac{\partial h}{\partial y} + \frac{\partial f}{\partial k} \frac{\partial k}{\partial h} \frac{\partial h}{\partial y} \right) \quad (9)$$

and after a lengthy algebraic manipulation, Eq. (7) becomes

$$\tilde{\phi}_{,tt} - \nabla \cdot (CC_g \nabla \tilde{\phi}) + (\omega^2 - k^2 CC_g) \tilde{\phi} + \omega^2 \{R_1 (\nabla h)^2 + R_2 \nabla^2 h\} \tilde{\phi} = 0, \quad (10)$$

where

$$R_1 = \frac{1}{\cosh^2 kh} (W_1 I_1 + W_2 I_2 + W_3 I_3 + W_4 I_4 + W_5 I_5 + W_6) \quad (11)$$

$$R_2 = \frac{1}{\cosh^2 kh} (U_1 I_1 + U_2 I_2 + U_3 I_3). \quad (12)$$

The expressions of W_i , U_i , and I_i are given in Appendix A. The coefficients R_1 and R_2 could be considerably simplified as in Massel (1994) and Chamberlain and Porter (1995).

For a monochromatic wave, the model equation becomes

$$\nabla \cdot (CC_g \nabla \tilde{\phi}) + k^2 CC_g \tilde{\phi} - \omega^2 \{R_1 (\nabla h)^2 + R_2 \nabla^2 h\} \tilde{\phi} = 0 \quad (13)$$

which is the same as the equation for propagating wave mode developed by Massel (1993) except for minor algebraic errors in W_1 and W_2 of the Massel's equation. It should also be noted that for a monochromatic wave Eq. (7) reduces to the modified mild-slope equation proposed by Chamberlain and Porter (1995). Conclusively the time-invariant form of the present equation is the same as the extended refraction–diffraction equation of Massel and the modified mild-slope equation of Chamberlain and Porter. This equation has been used by Suh and Park (1995) for the prediction of reflection coefficient of a composite-type perforated-wall caisson breakwater including the effect of a rubble mound foundation with a relatively steep fore slope.

2.2. Lagrangian formulation

The variational principle governing irrotational fluid motion is given by (Luke, 1967)

$$\delta \int_t \int_x \int_y L(x, y, t, \phi, \nabla \phi, \phi_t, \eta) dy dx dt = 0, \quad (14)$$

where η is the free surface displacement. The preceding equation implies that the integral of the Lagrangian L over all space and time is stationary with respect to small variation. Luke (1967) gives

$$L = \int_{-h}^{\eta} \frac{P}{\rho} dz = - \int_{-h}^{\eta} \left[\phi_t + \frac{1}{2} (\nabla \phi)^2 + \frac{1}{2} \phi_z^2 + gz \right] dz \quad (15)$$

Retaining the terms in second order in the Lagrangian L and using the expression for ϕ in Eq. (4), after neglecting the nonpropagating evanescent modes, we get

$$\begin{aligned}
 -L = & \eta \tilde{\phi}_t + \frac{1}{2} \frac{CC_g}{g} (\nabla \tilde{\phi})^2 + \frac{1}{2} \frac{\omega^2 - k^2 CC_g}{g} \tilde{\phi}^2 + \frac{1}{2} \int_{-h}^0 (\nabla f)^2 dz \tilde{\phi}^2 \\
 & + \int_{-h}^0 f \nabla f dz \tilde{\phi} \nabla \tilde{\phi} + \frac{1}{2} g \eta^2.
 \end{aligned} \quad (16)$$

The stationariness of L with respect to η gives

$$\tilde{\phi}_t = -g\eta \quad (17)$$

which is the linearized dynamic free surface boundary condition. The stationariness of L with respect to $\tilde{\phi}$, after integrating by parts the fifth term on the right side of Eq. (16) and using the Leibnitz rule, gives

$$\eta_t = -\nabla \cdot \left(\frac{CC_g}{g} \nabla \tilde{\phi} \right) + \frac{\omega^2 - k^2 CC_g}{g} \tilde{\phi} - \left(\nabla h \cdot [f \nabla f]_{z=-h} + \int_{-h}^0 f \nabla^2 f dz \right) \tilde{\phi}. \quad (18)$$

The terms in the last parenthesis of the preceding equation is equivalent to the terms in the last parenthesis of Eq. (7). Therefore, the preceding equation can be written as

$$\eta_t = -\nabla \cdot \left(\frac{CC_g}{g} \nabla \tilde{\phi} \right) + \frac{\omega^2 - k^2 CC_g}{g} \tilde{\phi} + \frac{\omega^2}{g} \{ R_1 (\nabla h)^2 + R_2 \nabla^2 h \} \tilde{\phi}. \quad (19)$$

Eqs. (17) and (19) constitute a canonical form of time-dependent wave equations on the bottom with rapid depth variation. The terms in the brace of the preceding equation are $O((\nabla h)^2)$ and $O(\nabla^2 h)$ and were neglected in the equation of Radder and Dingemans (1985). The surface elevation η may be eliminated from Eqs. (17) and (19) in order to obtain Eq. (10), proving the equivalence of the two models which were developed by different methods.

3. Numerical examples

In order to validate the capability of the derived wave equation in the case of rapid depth variation, we first apply the time-invariant form of the equation (i.e., Eq. (13)) to the problem of reflection of monochromatic waves from a plane slope with different inclination, which has been tested by Booij (1983) to investigate the accuracy of the mild-slope equation with respect to bottom slope. Secondly, the equation is applied to the simulation of the resonant Bragg reflection of monochromatic waves due to singly and doubly periodic ripple patch, for which experimental data have been presented by Davies and Heathershaw (1984) and Guazzelli et al. (1992), respectively. Finally, a numerical example of the transmission of random waves over a periodic ripple bed is presented to demonstrate the applicability of the time-dependent wave equation to the simulation of random waves on rapidly varying topography.

For all the problems mentioned above, the bottom contours are straight and parallel to each other. For a monochromatic wave propagating over a straight and parallel bottom contour, Massel (1993) showed that Eq. (13) could be reduced to an ordinary differential equation with the upwave and downwave boundary conditions, which could be approximated by a system of linear equations, $\mathbf{A} \cdot \mathbf{x} = \mathbf{b}$, where \mathbf{A} is a tridiagonal band type matrix, \mathbf{x} is a column vector, and \mathbf{b} is also a column vector. The derivation of this equation is referred to Massel (1993). For the simulation of the propagation of random waves, the Adams–Moulton predictor–corrector method is used to solve Eqs. (17) and (19), which will be explained later in Section 3.3.

3.1. Wave reflection from a plane slope

By numerical computation for the reflection coefficient of a monochromatic wave normally incident on a plane slope, each end of which is connected to a constant-depth region, Booij (1983) has shown that the mild-slope equation gives accurate results up to 1:3 slope through comparison with a finite element numerical model. The wave period in the Booij's test was 2 s and the water depths on the upwave and downwave sides of the slope were 0.6 and 0.2 m, respectively, so that the difference of the water depth between the two constant-depth regions was 0.4 m.

Booij's finite element model solution, however, covers the slope range steeper than about 1:3 and no data is provided for the milder slopes. In order not only to examine the performance of the present equation but also to re-assess the accuracy of the mild-slope equation, we constructed a finite element model for the Booij's problem. An example of the finite element mesh is shown in Fig. 1 for the slope of 1:3. The finite element model is also based on linear potential wave theory. The near-field solution including the inclined slope was discretized by 8 noded isoparametric elements with quadratic shape functions. The far-field region was modeled using infinite elements whose shape function was derived from the usage of the progressive and first evanescent wave components in the analytical boundary series solutions (see Park et al., 1991). The shape function satisfies the radiation boundary condition at infinity. To properly model the behavior of the scattered waves, the infinite elements on the upwave and downwave sides were located at distances five times the constant water depth from both ends of the slope. The finite-difference model domain for the present equation and the mild-slope equation was taken the same as that for the finite element model as shown in Fig. 1 and

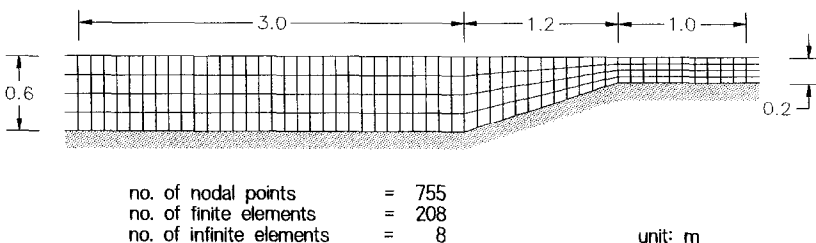


Fig. 1. Finite element mesh for the bottom slope of 1:3 of the Booij (1983) problem.

it was divided by 999 equally spaced intervals in the direction of wave propagation without regard to the bottom slope.

Fig. 2 compares the present equation, the mild-slope equation and the finite element model results. The abscissa, b , in the figure indicates the horizontal length of the plane slope normal to the wave crest lines. First it should be mentioned that for the relatively steep slope range our FEM model results are almost the same as the Booij's FEM model results in which triangular elements were used. It is shown that the present model gives reflection coefficients very close to those of the finite element model and the reflection coefficient becomes stable even for very steep slope, while the mild-slope equation underpredicts the reflection coefficient for steeper slopes. In the limiting case of the vertical step (i.e., $b = 0$), the finite element model gives the reflection coefficient of 0.228, which is not so different from the value of 0.225 for $b = 0.1$ m. Even for very mild slopes, the present equation and the mild-slope equation show some difference, and results of the finite element model coincide with the present equation rather than the mild-slope equation.

It has been well known that the mild-slope equation gives accurate results up to 1:3 slope. However, the results shown in Fig. 2 indicate that this is not true. It should be noted that the bottom configuration of the Booij's test includes the effects of slope discontinuity at both ends of the slope as well as the bottom slope. The former effect may be represented by the bottom curvature term of the present equation, which is nonzero only at the ends of the slope in the Booij's problem (The bottom curvature at the ends of the slope is approximately given by central-differencing $\partial^2 h / \partial x^2$, i.e., $\partial^2 h / \partial x^2 = [h(x + \delta x) - 2h(x) + h(x - \delta x)] / (\delta x)^2$ where δx is the grid spacing in the wave propagation direction.) Thus, if we want to assess the accuracy of the mild-slope equation merely for bottom slope, we have to use the mild-slope equation including the bottom curvature term, i.e., Eq. (13) with $R_1 = 0$. This result is shown in Fig. 2 by a dash-dotted line, which gives somewhat larger reflection coefficient than the

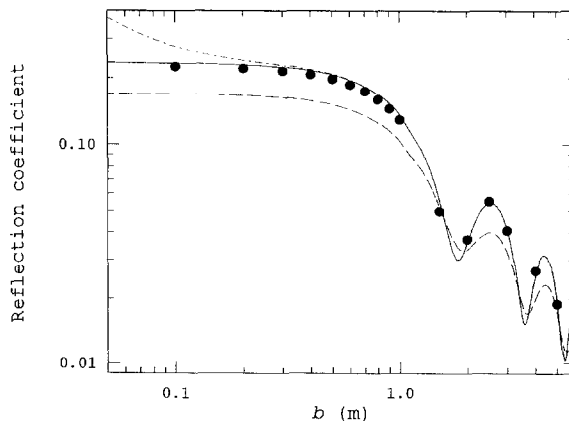


Fig. 2. Reflection coefficient versus horizontal length of a plane slope; ● = finite element model, — = present equation, --- = mild-slope equation, - · - · = mild-slope equation including the bottom curvature effect.

present equation for steeper slopes but is almost identical with the present equation for milder slopes.

Recently Porter and Staziker (1995) have tested the mild-slope equation and the modified mild-slope equation for this problem, showing that these equations do not ensure continuity of mass flow at locations where the bed slope is discontinuous and the use of interfacial jump conditions at such locations improves the accuracy of these equations. The solution technique of Porter and Staziker is different from that of the present study. In the present study the whole domain including the slope and the horizontal bed regions was modeled as one, but Porter and Staziker divided the domain into three regions (i.e., two horizontal bed regions and the sloping bed region) and imposed matching conditions at the interfaces between neighboring regions. Therefore, in the solution of Porter and Staziker, the effect of bottom curvature is not included directly in the calculation but it is included through the use of interfacial jump condition. A comparison between Fig. 2 and the corresponding figure in the Porter and Staziker paper (Fig. 2a) shows that the two results are almost identical. This means that the effect of the use of the interfacial jump conditions in the Porter and Staziker solution is equivalent to the inclusion of the bottom curvature term in our solution. Another important thing we can see in Fig. 2 is that when only the bottom slope is concerned the mild-slope equation can give accurate results up to 1:1 slope rather than 1:3 slope. But it should not be overlooked that the inclusion of the bottom curvature term played an important role in improving the accuracy of the mild-slope equation for milder slopes.

3.2. Resonant Bragg reflection of monochromatic waves

The problem of reflection of surface waves by a patch of periodic bottom undulations has recently received a great deal of attention. When surface waves are normally incident on a region of long-crested periodic bottom undulation, a significant amount of incident wave energy is reflected at the point where the wavenumber of the periodic bottom undulation (K) is twice the wavenumber of the surface wave (k), that is, $2k/K = 1$. This wave reflection, which has been known as Bragg reflection, has been studied in coastal engineering because it may either provide a measure to protect shore face from the full impact of the waves by partially reflecting incident waves having the appropriate wavelength or explain the mechanism of the growth of periodic sand bars due to the interaction between the surface wave and erodible sand bed in nearshore regions.

The Bragg reflection of surface waves has been studied both by laboratory experiments and through theoretical or numerical models. Davies and Heathershaw (1984) reported experimental data for the reflection of waves due to singly sinusoidal ripple patches with different numbers of ripples. These data have been used for comparison with various numerical models by a number of researchers including Davies and Heathershaw (1984) themselves, Dalrymple and Kirby (1986), Kirby (1986), O'Hare and Davies (1993), Massel (1993) and Chamberlain and Porter (1995). Similar laboratory experiments were reported by Hara and Mei (1987), Benjamin et al. (1987) and Kirby and Anton (1990). Especially the experimental data of Kirby and Anton revealed that the second-order Bragg reflection occurred in the vicinity of $2k/K = 2$ in addition

to the main Bragg resonant peak in the vicinity of $2k/K = 1$ and that the resonant peaks were shifted towards smaller values of $2k/K$ compared with the values of $2k/K = 1$ and 2 which were predicted by the lowest-order theories of Miles (1981) and Mei (1985).

A more intensive study on the higher-order Bragg reflection was recently made by Guazzelli et al. (1992), who carried out laboratory experiments for reflection of surface waves by doubly sinusoidal ripple beds. In the case of a bed consisting of the superposition of two sinusoids having different wavenumbers, K_1 and K_2 ($K_2 > K_1$), Guazzelli et al. showed that the first-order Bragg reflections occurred in the vicinities of $2k = K_1$ and K_2 while the second-order reflections were revealed in the vicinities of $2k = 2K_1$, $2K_2$, $K_2 + K_1$ (harmonic Bragg reflections) and $2k = K_2 - K_1$ (sub-harmonic Bragg reflection). They also showed that the center of each resonant peak was slightly shifted towards a smaller wavenumber than the predicted value given above.

First, the derived equation is compared with the experimental data of Davies and Heathershaw (1984) for the reflection of monochromatic waves by a singly periodic ripple patch. Secondly, the equation is applied to the simulation of the higher-order Bragg reflections due to doubly sinusoidal ripple beds for which experimental data were reported by Guazzelli et al. (1992).

The test conditions of the Davies and Heathershaw (1984) experiment are summarized in Table 1, in which A is the ripple amplitude, λ is the ripple wavelength, n is the number of ripples, and h_c is the water depth in the region of flat bottom. The water depth is given by

$$h(x) = \begin{cases} h_c, & x \leq 0 \\ h_c - A \sin(Kx), & 0 \leq x \leq n\lambda \\ h_c, & x \geq n\lambda \end{cases} \quad (20)$$

Reflection coefficients computed by the present model are given by solid lines in Figs. 3–5 for the beds D_1 , D_2 , and D_3 , respectively, in comparison with the experimental data. Also shown in these figures are the results obtained using the mild-slope equation (dashed lines). As shown in Figs. 3 and 4, for the beds D_1 and D_2 for which waves are relatively long compared to the water depth, the results of the mild-slope equation are in close agreement with the results of the present model. Fig. 5 shows that for the bed D_3 the mild-slope equation, while correctly positioning the resonant reflection, completely fails to predict its magnitude. In this case, waves are relatively

Table 1
Test conditions of the experiment of Davies and Heathershaw (1984)

Bed	A (cm)	$\lambda(K)$ (cm)	n	h_c (cm)
D_1	5	100 (0.0628 cm^{-1})	2	15.6
D_2	5	100 (0.0628 cm^{-1})	4	15.6
D_3	5	100 (0.0628 cm^{-1})	10	31.3

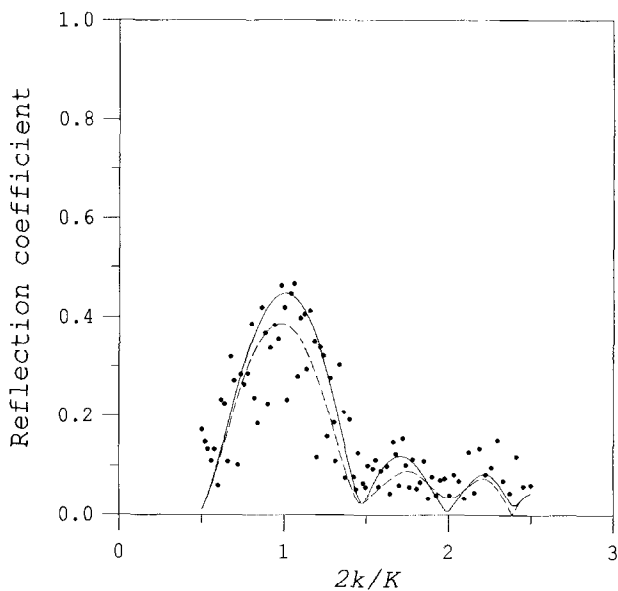


Fig. 3. Comparison of the present equation and the mild-slope equation with the experimental data of Davies and Heathershaw (1984) for the bed D_1 ; — = present equation, --- = mild-slope equation, ● = experimental data.

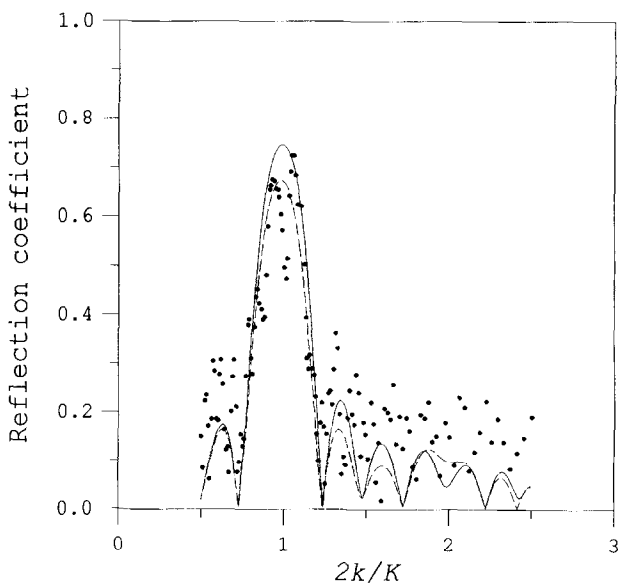


Fig. 4. Same as Fig. 3, but for the bed D_2 .

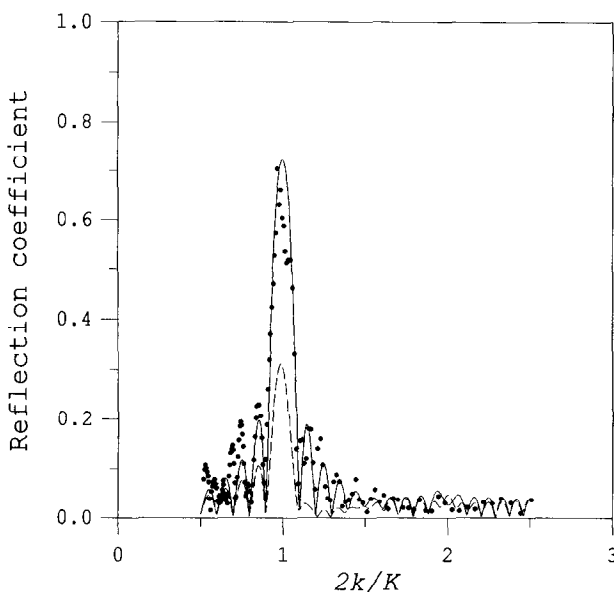


Fig. 5. Same as Fig. 3, but for the bed D_3 .

short compared to the water depth so that violation may be made on the assumption of the mild-slope equation that the depth must vary slowly over a wavelength. The present model which includes the higher-order bottom effect terms, however, describes the resonant peak very well. The scattering of the experimental data and the disagreement between theory and data become apparent for the beds D_1 and D_2 probably because of the reflection from the beach at the end of the wave channel. Davies and Heathershaw (1984) indicated that the reflection coefficients for the beach were of the order of 0.1 or less for the bed D_3 , but those for the beds D_1 and D_2 were of the order of 0.2.

The next example of the Bragg reflection is that due to doubly sinusoidal ripple beds for which the experimental data of Guazzelli et al. (1992) are available. The test conditions of the experiment are summarized in Table 2, in which A is the ripple amplitude taken the same for both ripples of different wavelengths, λ_1 and λ_2 are the wavelengths of the longer and shorter ripples, respectively, $m = \lambda_1/\lambda_2 = K_2/K_1$ is the

Table 2

Test conditions of the experimental of Guazzelli et al. (1992)

Bed	A (cm)	$\lambda_1(K_1)$ (cm)	$\lambda_2(K_2)$ (cm)	m	l (cm)	h_c (cm)
G_1	1	12 (0.52 cm^{-1})	6 (1.05 cm^{-1})	2	48, 192	2.5, 3, 4
G_2	0.5	6 (1.05 cm^{-1})	4 (1.57 cm^{-1})	1.5	48	2.5, 3, 4
G_3	1	6 (1.05 cm^{-1})	4 (1.57 cm^{-1})	1.5	48	2.5, 3, 4

ratio of the larger and smaller ripple wavelengths, l is the total length of the ripple patch, and h_c is the water depth in the region of flat bottom. The water depth is given by

$$h(x) = \begin{cases} h_c, & x \leq 0 \\ h_c - A[\sin(K_1 x) + \sin(mK_1 x)], & 0 \leq x \leq l \\ h_c, & x \geq l \end{cases} \quad (21)$$

For the bed G_1 , the larger ripple wavelength is twice the smaller ripple wavelength so that the subharmonic Bragg resonance peak at $k = (K_2 - K_1)/2$ would coincide with the Bragg peak due to the larger wavelength ripples at $k = K_1/2$. For the beds G_2 and G_3 , the larger ripple wavelength is 1.5 times the smaller ripple wavelength so that the subharmonic Bragg resonance peak would appear at the wavenumber smaller than that of the Bragg peak due to the larger wavelength ripples. For each bed, tests were made for three different water depths to examine the importance of relative ripple amplitude with respect to the water depth. In the present study, only the data corresponding to $h_c = 2.5$ and 4 cm are compared with the numerical model results because the data for $h_c = 3$ cm show intermediate behavior between these two extreme values as described in the paper of Guazzelli et al. (1992).

Fig. 6 shows the comparison between the measured reflection coefficients and the predictions of the present equation and the mild-slope equation for the bed, G_1 , with the total length of the ripple patch, $l = 48$ cm. The mild-slope equation gives erroneous results compared to the present equation, and as expected, the wave reflection in shallower water is much higher than deeper water. Also, in shallower water, the occurrence of harmonic Bragg reflections at $2k/K_1 = 3$ and 4 and the shifts of the Bragg resonance peaks towards smaller wavenumbers are obviously observed in both experiment and prediction. In deeper water, however, the shifts of the resonant peaks are minute and the harmonic Bragg resonances are predicted not to occur by the present equation even though the experimental data do not cover this range of wavenumbers.

Results obtained for the same bed G_1 but with a longer length of the ripple patch, $l = 192$ cm, are shown in Fig. 7. The features described above are again shown as far as the shift towards a smaller wavenumber and the occurrence of the harmonic Bragg reflection are concerned. However, many more oscillations are present between the main resonant peaks of which the amplitude increases and the peak width decreases compared with those of the shorter length of ripple patch (Fig. 6). This feature has also been observed for singly sinusoidal ripple beds by Davies and Heathershaw (1984).

Fig. 8 shows the results for the bed G_2 for which the subharmonic Bragg resonant peak is expected to occur in the vicinity of $2k/K_1 = 0.5$ in addition to the main and harmonic resonant peaks at larger wavenumbers. Again the wave reflection in shallower water is much higher than deeper water. In this case, however, the shifts of the resonant peaks towards smaller wavenumbers are not prominent in both water depths probably because the ripple amplitude is smaller than that of the bed G_1 . The subharmonic resonant peak is predicted by the present equation though it somewhat underpredicts the experimental data.

Fig. 9 shows the results for the bed G_3 which is the same as G_2 except for the larger

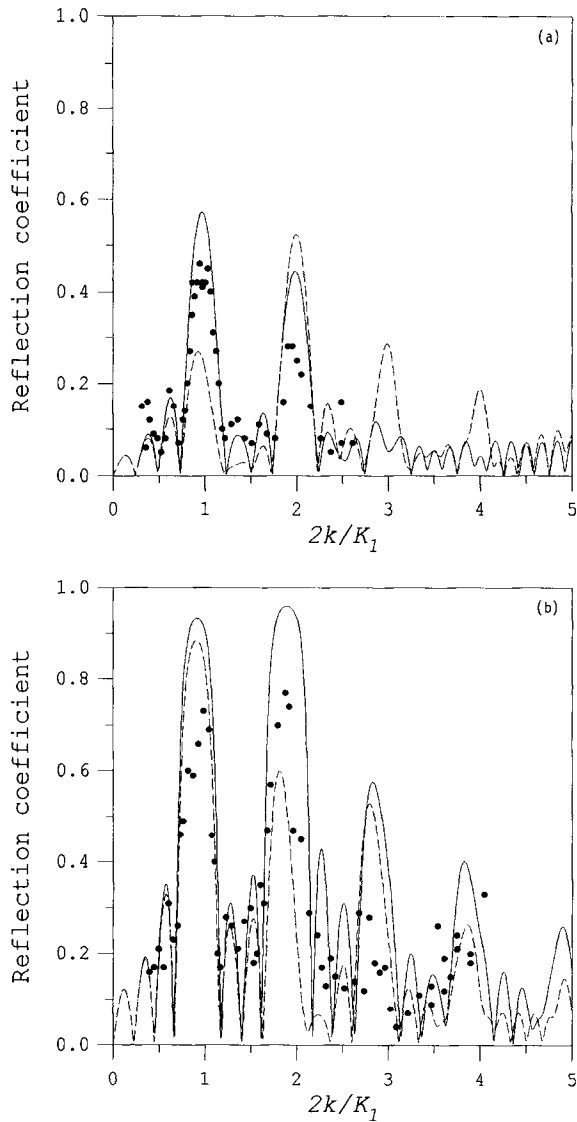


Fig. 6. Comparison of the present equation and the mild-slope equation with the experimental data of Guazzelli et al. (1992) for bed G_1 with $l = 48$ cm; — = present equation, --- = mild-slope equation, ● = experimental data. (a) $h_c = 4$ cm, (b) $h_c = 2.5$ cm.

ripple amplitude. The magnitude of the subharmonic resonant peak is comparable to the main peaks, and in shallower water the prominent harmonic resonant peaks at larger wavenumbers are predicted though experimental data are not available in this range of wavenumbers. The shifts of the resonant peaks towards smaller wavenumbers are also observed in both experiment and prediction.

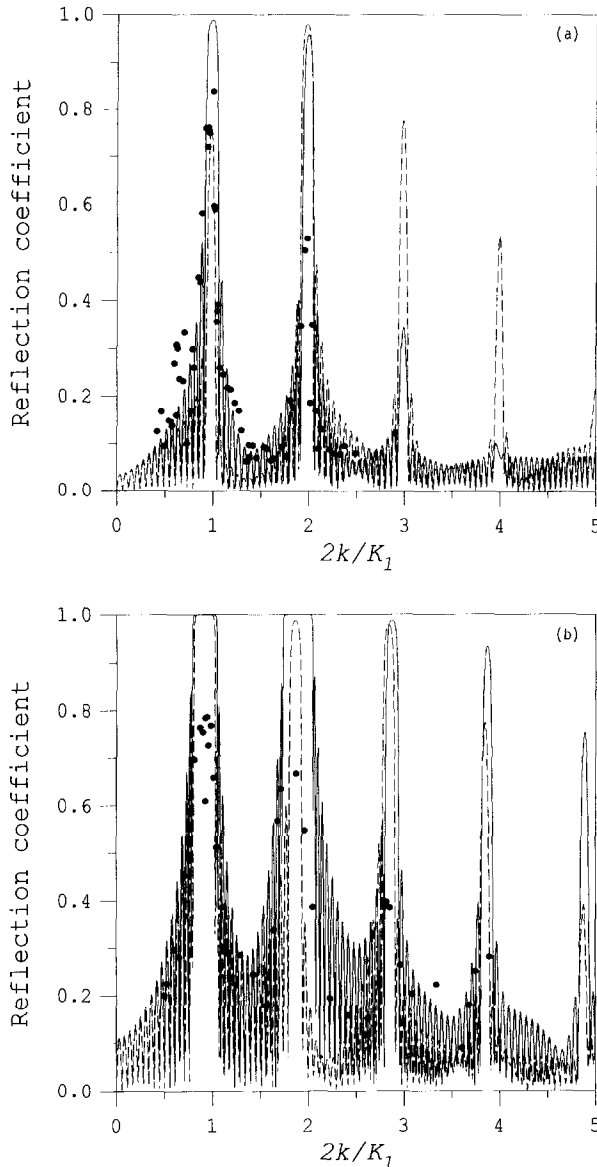


Fig. 7. Same as Fig. 6, but for the bed G_1 with $l = 192$ cm.

The experimental data of Guazzelli et al. (1992) have been used for comparison with the successive application matrix model of O'Hare and Davies (1992) and the extended mild-slope equation model of Kirby (1986) by O'Hare and Davies (1993). Guazzelli et al. (1992) also compared the experimental data with their own numerical model which is based on the approach of Takano (1960). The model of Guazzelli et al. (1992) is similar

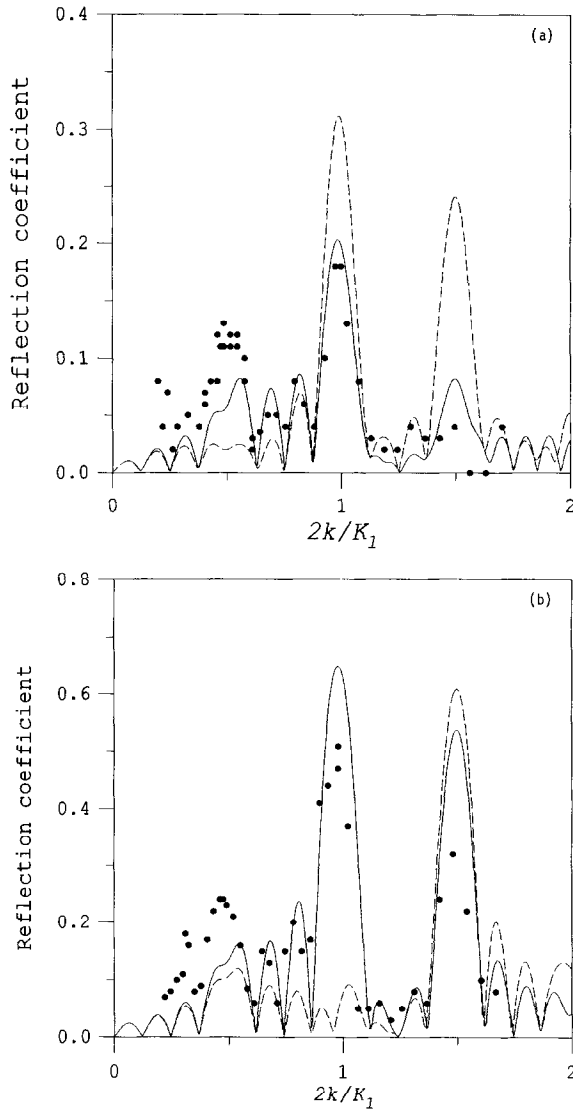


Fig. 8. Same as Fig. 6, but for the bed G_2 .

to that of O'Hare and Davies (1992) in that the bed is discretized into a series of horizontal shelves but differs in that it can include not only the propagating wave mode but also the nonpropagating (or evanescent) wave modes generated at each discontinuity with neighboring steps. Both Guazzelli et al. (1992) and O'Hare and Davies (1993) concluded that the inclusion of the evanescent wave modes has the general effect of shifting the resonance peaks towards smaller wavenumbers and reducing the size of all the higher-order resonances, except for the subharmonic resonance which is enhanced.

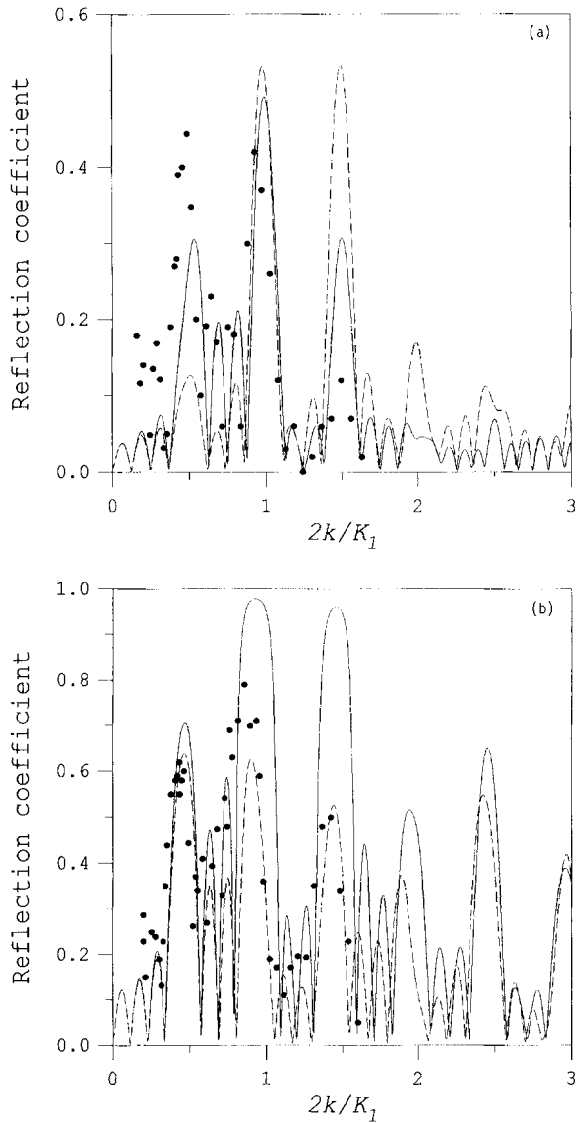


Fig. 9. Same as Fig. 6, but for the bed G_3 .

In fact, Guazzelli et al. (1992) demonstrated such effects of the evanescent wave modes by comparing their model with the experimental data. As a result, the present model which does not include the evanescent modes also underpredicts the subharmonic resonant peaks as shown in Figs. 8 and 9. In the vicinity of the subharmonic resonant peaks, the result of the present model is comparable to those of the matrix model of O'Hare and Davies (1993) and the model of Guazzelli et al. (1992) without the inclusion of the evanescent wave modes.

3.3. Transmission of random waves over a ripple patch

So far we tested the derived equation for the problems of monochromatic waves. One of the advantages of a time-dependent wave equation is that it can be used for the simulation of random waves. However, experimental data for random waves propagating over rapidly varying topography are rare. Therefore, here we test numerically the time-dependent equations for the case of unidirectional random waves normally incident on a finite ripple patch. The test conditions are chosen to be the same as the bed D_3 of the Davies and Heathershaw (1984) experiment (cf. Table 1) for which a marked discrepancy was observed between the results of the present equation and the mild-slope equation for the case of a monochromatic wave. For monochromatic waves, we calculated the wave reflection from the ripple patch as in Section 3.2. Even for random waves, it may be possible to calculate the wave reflection if we use the technique for separation of incident and reflected waves (Mansard and Funke (1980), for example). However, some errors may be somehow involved in this procedure. In the present test of random waves, therefore, we examine wave transmission over the ripples rather than wave reflection.

The TMA shallow-water spectrum (Bouws et al., 1985) is used as the input target spectrum:

$$S(f) = \alpha g^2 (2\pi)^{-4} f^{-5} \exp\left[-1.25(f/f_p)^{-4}\right] \gamma^{\exp[-(f/f_p - 1)^2 / 2\sigma^2]} \phi_k(f, h), \quad (22)$$

where α is a spectral parameter, γ is the peak enhancement factor, σ is the spectral width parameter ($\sigma = \sigma_a$ if $f \leq f_p$ and $\sigma = \sigma_b$ if $f > f_p$; $\sigma_a = 0.07$ and $\sigma_b = 0.09$ were used), and finally the Kitaigorodskii shape function, $\phi_k(f, h)$, is approximately given by

$$\phi_k(f, h) = \begin{cases} 0.5\omega_h^2, & \omega_h < 1 \\ 1 - 0.5(2 - \omega_h)^2, & 1 \leq \omega_h \leq 2 \\ 1, & \omega_h > 2, \end{cases} \quad (23)$$

where $\omega_h = 2\pi f(h/g)^{1/2}$.

Two cases of numerical tests are conducted: one with narrow frequency spectrum ($\gamma = 20$) and the other with broad frequency spectrum ($\gamma = 2$). $\alpha = 7.57 \times 10^{-4}$ was used in both cases. The peak frequency, f_p , was 0.76 Hz in both cases, for which $2k_p/K$ is 1.0 and thus significant wave reflection from the ripple patch is expected in the vicinity of the peak frequency.

Before starting the test of the time-dependent wave equations, we calculated the transmission coefficient separately for each frequency of the TMA spectrum using the time-invariant form of the present equation, the mild-slope equation, and the finite element model described in Section 3.1. The transmitted wave spectra calculated from the three methods are shown in Figs. 10 and 11 for the narrow and broad spectrum, respectively, along with the incident wave spectrum. The transmitted wave spectra of both the FEM solution and the present equation show significant reduction in the vicinity of the peak frequency compared with the input spectrum because of wave

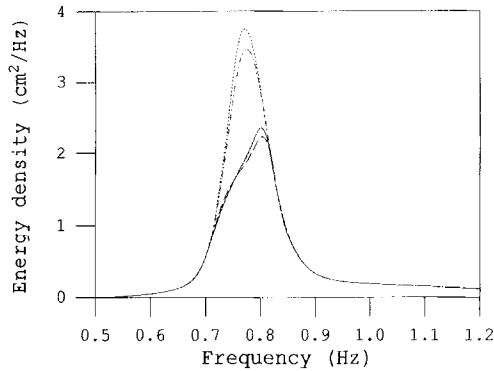


Fig. 10. Incident and transmitted wave spectra of narrow-banded TMA spectrum; --- = incident wave, — = FEM solution, ··· = time-invariant form of present equation, - · - = mild-slope equation.

reflection by the ripples. However, the mild-slope equation yields only a slight reduction near the peak frequency, as expected. The FEM solution and the present equation show a little difference probably because the FEM solution includes the evanescent wave components as well as the progressive one. The FEM solution may be regarded as an exact solution for linear random waves. Therefore, in the following, the solutions of the time-dependent wave equations will be compared against the FEM solution.

In solving the time-dependent wave equations (17) and (19), the wave parameters such as ω , k , C and C_g are chosen to be the values corresponding to the carrier frequency \bar{f} on the assumption of a narrow-banded frequency spectrum. The wave parameters would become inaccurate for the wave components far from the carrier frequency. Since the TMA spectrum has a long tail in the high frequency region, especially for the narrow spectrum, the input spectrum was confined within a certain frequency range. For the narrow spectrum, both the lower and upper cutoff frequencies were taken as the frequency at which the energy density is 5% of that at the spectral

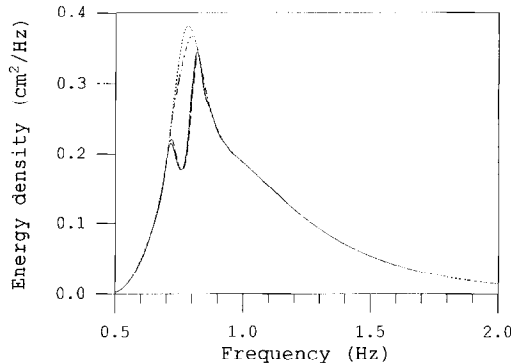


Fig. 11. Incident and transmitted wave spectra of broad-banded TMA spectrum; --- = incident wave, — = FEM solution, ··· = time-invariant form of present equation, - · - = mild-slope equation.

Table 3
Test conditions of transmission of random waves over a ripple patch

Spectrum	Number of bands	Band order	f_{\min} (Hz)	\bar{f} (Hz)	f_{\max} (Hz)
Narrow	1	1st	0.67	0.79	1.00
		2	0.67	0.75	0.78
	3	2nd	0.78	0.83	1.00
		1st	0.67	0.74	0.76
		2nd	0.76	0.78	0.80
		3rd	0.80	0.85	1.00
Broad	1	1st	0.59	0.98	1.63
	2	1st	0.59	0.78	0.92
		2nd	0.92	1.18	1.63
	3	1st	0.59	0.74	0.82
		2nd	0.82	0.93	1.06
		3rd	1.06	1.28	1.63

peak so that the confined range of the spectrum (between 0.67 and 1.00 Hz) covers 83% of the total energy. For the broad spectrum, the energy density at both the lower and upper cutoff frequencies was 10% of the peak spectral density, and the confined range of the spectrum (between 0.59 and 1.63 Hz) covers 90% of the total energy. The significant wave height calculated from the wave energy within the confined frequency range was 2.54 and 1.58 cm for the narrow and broad spectrum, respectively.

In order to obtain still better accuracy, the selected frequency range could be divided into several bands and each of them could be modeled with a representative carrier frequency. In the present study, three cases of different number of frequency bands (one, two, and three) are examined. The division of frequency bands is made so that each band contains the same energy, and in each frequency band the carrier frequency is selected as the weight-averaged frequency. Details of the test conditions are given in Table 3.

The schematic diagram of the numerical test is shown in Fig. 12, in which L_p is the wavelength corresponding to the peak frequency, f_p , of the input frequency spectrum. A time-series of normally incident random waves is generated internally inside the model

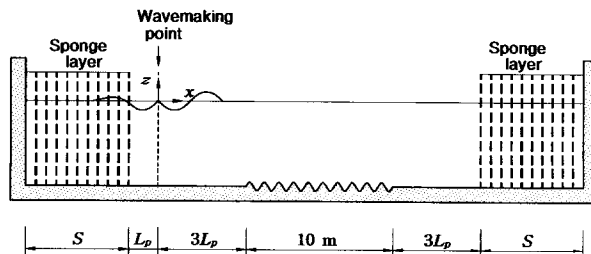


Fig. 12. Schematic diagram of the model domain for the numerical calculation of random waves propagating over a ripple patch.

boundaries while the waves reflected from the ripple patch are permitted to freely pass across the wavemaker so that unwanted addition of wave energy inside the model domain can be avoided. This technique was previously developed by Larsen and Dancy (1983) for the Boussinesq equation and was used by Madsen and Larsen (1987) for the Copeland (1985) equation. They argued that the velocity of disturbances caused by the incident wave is the phase speed from the viewpoint of mass transport. Lee and Suh (1997) applied this technique to a monochromatic wave in the Radder and Dingemans (1985) equations and found that the resulting amplitude of the incident wave is different from the desired amplitude by the ratio of C/C_g . However, from the viewpoint of energy transport, they could obtain the desired wave amplitude for the Radder and Dingemans model. The viewpoint of energy transport suggests the use of the energy velocity for the velocity of the disturbances. The energy velocity can be obtained using the geometric optics approach. In the present model, the energy velocity is given by (Lee and Suh, 1997)

$$C_e = \bar{C}_g \frac{\bar{\omega}}{\omega} \sqrt{1 + \frac{\bar{C}}{\bar{C}_g} \left(\left(\frac{\omega}{\bar{\omega}} \right)^2 - 1 \right)}, \quad (24)$$

where the overbar is associated with the carrier frequency \bar{f} .

Waves are generated internally by adding the water surface elevations of incident wave to the computed ones at the wave generation line. The value of η^* added to the surface elevation at each time step at the wave generation line is given by

$$\eta^* = 2 \tanh(f_p t) \sum_j \frac{C_{cj} \Delta t}{\Delta x} A_j e^{i(k_j x - \omega_j t + \epsilon_j)} = 2 \tanh(f_p t) \frac{\bar{C}_g \Delta t}{\Delta x} \sum_j \tilde{A}_j e^{i(k_j x - \omega_j t + \epsilon_j)}, \quad (25)$$

where

$$\tilde{A}_j = A_j \frac{\bar{\omega}}{\omega_j} \sqrt{1 + \frac{\bar{C}}{\bar{C}_g} \left(\left(\frac{\omega_j}{\bar{\omega}} \right)^2 - 1 \right)}. \quad (26)$$

A_j is the amplitude of incident wave with the local angular frequency ω_j , Δx and Δt are the grid spacing and time step, respectively, ϵ_j is the random phase, and the term $\tanh(f_p t)$ is added for slow start of wave generation.

A time-series of free surface elevation of random waves was generated by the inverse Fourier transform of the TMA spectrum. The time step for the inverse Fourier transform was $T_p/41$ and the total number of time step was 16,384 so that the total time for wave generation was $399.61T_p$. After $399.61T_p$, waves were generated repeatedly from the start.

A sponge layer was placed at both upwave and downwave boundaries to minimize wave reflection from the boundaries by dissipating wave energy inside the sponge layers. The thickness of the sponge layer, S , was taken as 2.5 times the longest

wavelength of the waves to be modeled, being found to reduce the magnitude of the incident wave to almost zero at the boundaries. Eq. (17) is modified to

$$\tilde{\phi}_t = -g\eta - w\tilde{\phi}, \quad (27)$$

where

$$w = \begin{cases} 0, & \text{outside sponge layer} \\ \omega_{\max} \left(\frac{e^{d/s} - 1}{e - 1} \right), & \text{inside sponge layer,} \end{cases} \quad (28)$$

where ω_{\max} is the maximum angular frequency of the waves to be modeled and d is the distance from the starting point of the sponge layer. The damping coefficient w increases exponentially from zero at the starting point of the sponge layer to ω_{\max} at the end.

Eqs. (19) and (27) are discretized by a fourth-order Adams–Moulton predictor–corrector method in time and by a three-point symmetric formula in space. The predictor step yields

$$\eta^{n+1} = \eta^n + \frac{\Delta t}{24} (55F^n - 59F^{n-1} + 37F^{n-2} - 9F^{n-3}) \quad (29)$$

$$\tilde{\phi}^{n+1} = \tilde{\phi}^n + \frac{\Delta t}{24} (55G^n - 59G^{n-1} + 37G^{n-2} - 9G^{n-3}) \quad (30)$$

and the corrector step yields

$$\eta^{n+1} = \eta^n + \frac{\Delta t}{24} (9F^{n+1} + 19F^n - 5F^{n-1} + F^{n-2}) \quad (31)$$

$$\tilde{\phi}^{n+1} = \tilde{\phi}^n + \frac{\Delta t}{24} (9G^{n+1} + 19G^n - 5G^{n-1} + G^{n-2}), \quad (32)$$

where the superscript n ($= 0, \dots, N$) denotes the value in the n th time step, and $F(\tilde{\phi})$ and $G(\tilde{\phi}, \eta)$ are the right-hand sides of Eqs. (19) and (27), respectively. All the values at the initial stage ($n = 0$) are set to be zero, i.e., $\eta^0 = \tilde{\phi}^0 = 0$. At both upwave and downwave boundaries, perfect reflection is assumed, i.e., $\tilde{\phi}_1 = \tilde{\phi}_2$ and $\tilde{\phi}_J = \tilde{\phi}_{J-1}$, where the subscript denotes the grid point when the model domain is discretized by J equidistant points. However, the effect of the reflection from these boundaries is negligibly small in the region of interest because the sponge layer significantly reduces the incoming waves.

The grid spacing Δx was chosen so that the local wave length is greater than $10\Delta x$ and a spatial resolution is guaranteed. The time step $\Delta t = T_p/328$ was chosen so that the Courant number $C_r = C_e \Delta t / \Delta x$ is less than 0.1 and a stable solution is guaranteed. Since the time step of $T_p/41$ was used for wave generation, linear interpolation was used to obtain the surface elevations of $\Delta t = T_p/328$ at the wavemaker.

Surface elevations were recorded at a point in the lee of the ripple patch to calculate the transmitted wave spectrum. In order to permit the slower-traveling high-frequency component waves to travel to the point of wave recording, the surface elevations were

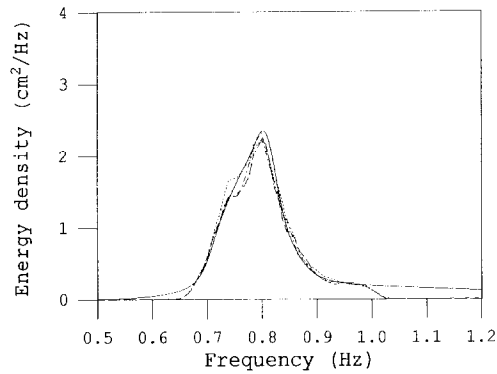


Fig. 13. Transmitted wave spectra calculated with different number of frequency bands using the present equation for narrow-banded TMA spectrum; --- = one band, -.-.- = two bands, .-.-. = three bands, ——— = FEM solution.

xxx

recorded from $50T_p$ to $449.61T_p$ with the sampling interval of $T_p/41$ so that the total number of samples was 16,384. In the spectral analysis of the data, the smoothing techniques presented in Otnes and Enochson (1978) were used. The 16,384 data points were processed in seven segments of 4,096 points per segment. These segments overlap by 50% for smoother and statistically more significant spectral estimates. The raw spectra were then ensemble-averaged. Further smoothing was made by band-averaging over five neighboring frequency bands. The total number of degrees of freedom is about 47 for final spectra.

Fig. 13 shows the comparison of the transmitted wave spectra calculated by the present time-dependent wave equations against the FEM solution for the case of narrow frequency spectrum. As mentioned previously, the FEM solution may be regarded as an exact solution for linear random waves. In the vicinity of the Bragg resonant frequency ($f = 0.76$ Hz), the solutions using different number of frequency bands show some

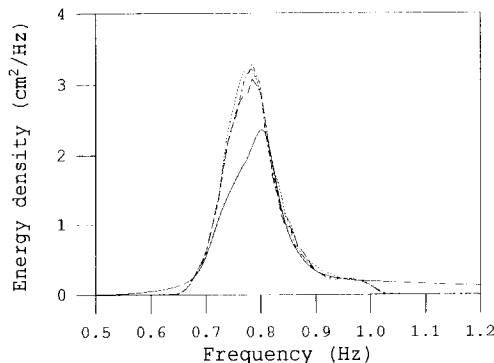


Fig. 14. Same as Fig. 13, but using the Radder and Dingemans (1985) equation.

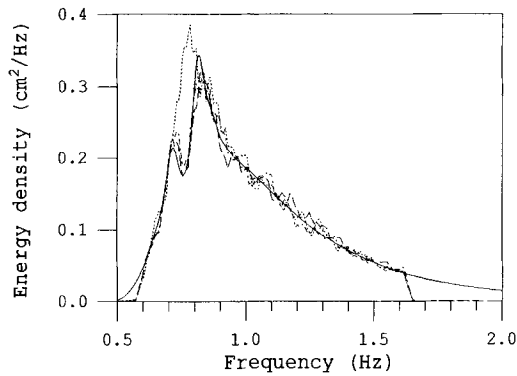


Fig. 15. Transmitted wave spectra calculated with different number of frequency bands using the present equation for broad-banded TMA spectrum; --- = one band, - - - = two bands, - · - · = three bands, — = FEM solution.

difference, but the overall shapes of the solutions do not change much with the number of frequency bands. As expected, the transmitted wave spectrum shows significant reduction compared with the input spectrum near the Bragg resonant peak, while most of the wave energy is transmitted over the ripples for the wave components whose frequency is far out of the resonant frequency. A similar plot is shown in Fig. 14 for the results obtained from the time-dependent mild-slope equations of Radder and Dingemans (1985). Again, in the vicinity of the Bragg resonant frequency, the solutions using different number of frequency bands show some difference, but as a whole the solutions are far from the exact solution (i.e., the FEM solution), predicting much larger wave transmission than the present solution or the FEM solution.

Fig. 15 shows the comparison of the transmitted wave spectra calculated by the present time-dependent wave equations against the FEM solution for the case of broad frequency spectrum. When using a single carrier frequency representing the whole frequency range, the solution does not detect the reduction of wave transmission near the

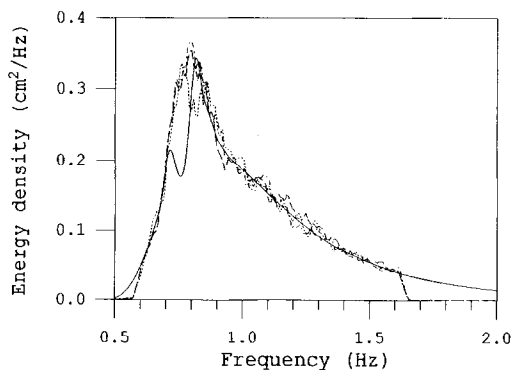


Fig. 16. Same as Fig. 15, but using the Radder and Dingemans (1985) equation.

Bragg resonant peak. As the number of frequency bands increases, the solution approaches the exact solution. Fig. 16 shows a similar plot using the results of the equations of Radder and Dingemans (1985). Again the solutions show large discrepancy from the exact solution.

4. Conclusion

Two time-dependent wave equations to include the effect of rapid depth variation have been developed by different theoretical approaches (Green's formula method and Lagrangian formulation), but the resulting equations have been shown to be identical. Without the higher-order bottom effect terms, the former and the latter reduce to the time-dependent mild-slope equations developed by Smith and Sprinks (1975) and Radder and Dingemans (1985), respectively. For a monochromatic wave, the developed equation reduces to the Massel's (1993) extended refraction–diffraction equation for propagating wave alone and the modified mild-slope equation by Chamberlain and Porter (1995), which in turn, without the higher-order bottom effect terms, reduces to the Berkhoff's mild-slope equation.

For the case of monochromatic waves, the capability of the equation developed for rapidly varying topography has been verified by applying it to waves propagating over a plane slope with different inclination (Booij's problem) and the resonant Bragg reflection of surface waves due to singly or doubly periodic bottom topography. Comparison with other numerical results or experimental data showed that the developed equation was capable of predicting the wave scattering phenomena which were undetected by the Berkhoff's mild-slope equation. It was also shown that when only the bottom slope is concerned the mild-slope equation can give accurate results up to 1:1 slope rather than 1:3 slope, which, until now, has been known as the limiting bottom slope for the proper application of the mild-slope equation. This, however, does not imply that further effort to improve the mild-slope equation is not necessary. In fact, in the Booij's test, the inclusion of the bottom curvature term played an important role in improving the accuracy of the mild-slope equation for milder slopes.

For random waves, the time-dependent wave equations have been numerically tested for the transmission (or the Bragg reflection inversely) of unidirectional random waves normally incident on a finite ripple patch. The solutions were compared against the finite element model solution which may be regarded as an exact solution for linear random waves. The feature of the Bragg reflection of random waves was found to be very similar to that of monochromatic waves, that is, the wave components whose frequency is nearly or exactly resonant with the bottom experience fairly significant reflection by the ripple patch, while the reflection is very small for the wave components whose frequency is far out of the resonant frequency.

The use of a single carrier frequency could give a reasonably accurate result in the case of a narrow spectrum, but when the spectrum is broad, accurate results could be obtained by dividing the frequency range into several bands and modeling each of them with a representative carrier frequency.

Finally, the present equation which does not include the nonpropagating evanescent

modes fails to predict quantitatively the higher-order Bragg resonances for doubly sinusoidal beds. Presently modification of the equation is being made to include the evanescent modes and the result will be reported in another paper.

Acknowledgements

Partial support for this research was provided by the Korea Ministry of Science and Technology through Project No. BSPN-00289. C.L. would like to thank the Korea Science and Engineering Foundation for the support through the post-doc program. The writers would like to thank Professor A.G. Davies of the University of Wales and Professor Max Belzons of Université de Provence for providing the experimental data for the Bragg reflection of surface waves.

Appendix A. Components of terms R_1 and R_2

$$W_1 = -2\lambda + 2\frac{k_h}{k} + 2\frac{khk_h}{\lambda} - 4\frac{\lambda hk_h}{k} + \frac{hk_{hh}}{k} + \frac{h^2 k_h^2}{\lambda} - 2\frac{\lambda h^2 k_h^2}{k^2} \quad (33)$$

$$W_2 = 2k - 2\frac{k_h}{\lambda} + 2hk_h \quad (34)$$

$$W_3 = 2k_h - \frac{k_{hh}}{\lambda} + 2\frac{hk_h^2}{k} \quad (35)$$

$$W_4 = -2\frac{kk_h}{\lambda} \quad (36)$$

$$W_5 = -\frac{k_h^2}{\lambda} \quad (37)$$

$$W_6 = 1 + \frac{hk_h}{k} \quad (38)$$

$$U_1 = 1 + \frac{hk_h}{k} \quad (39)$$

$$U_2 = -\frac{k}{\lambda} \quad (40)$$

$$U_3 = -\frac{k_h}{\lambda} \quad (41)$$

$$I_1 = \int_{-h}^0 \cosh^2 k(h+z) dz \quad (42)$$

$$I_2 = \int_{-h}^0 \cosh k(h+z) \sinh k(h+z) dz \quad (43)$$

$$I_3 = \int_{-h}^0 (h+z) \cosh k(h+z) \sinh k(h+z) dz \quad (44)$$

$$I_4 = \int_{-h}^0 (h+z) \cosh^2 k(h+z) dz \quad (45)$$

$$I_5 = \int_{-h}^0 (h+z)^2 \cosh^2 k(h+z) dz \quad (46)$$

$$k_h = \frac{\partial k}{\partial h} = - \frac{\lambda k}{\lambda h + \sinh^2 kh} \quad (47)$$

$$k_{hh} = \frac{\partial^2 k}{\partial h^2} = - \frac{\lambda k_h}{\lambda h + \sinh^2 kh} \left(2 + \frac{k + hk_h}{\lambda} \sinh 2kh \right) \quad (48)$$

$$\lambda = \frac{\omega^2}{g} = k \tanh kh$$

References

- Benjamin, T.B., Boczar-Karakiewicz, B., Pritchard, W.G., 1987. Reflection of water waves in a channel with corrugated bed. *J. Fluid Mech.* 185, 249–274.
- Berkhoff, J.C.W., 1972. Computation of combined refraction–diffraction. In: *Proc. 13th Coastal Eng. Conf., Vancouver*, Vol. 1, pp. 471–490.
- Booij, N., 1983. A note on the accuracy of the mild-slope equation. *Coastal Eng.* 7, 191–203.
- Bouws, E., Günther, H., Rosenthal, W., Vincent, C.L., 1985. Similarity of the wind wave spectrum in finite depth water 1. Spectral form. *J. Geophys. Res.* 90 (C1), 975–986.
- Chamberlain, P.G., Porter, D., 1995. The modified mild-slope equation. *J. Fluid Mech.* 291, 393–407.
- Copeland, G.J.M., 1985. A practical alternative to the mild-slope wave equation. *Coastal Eng.* 9, 125–149.
- Dalrymple, R.A., Kirby, J.T., 1986. Water waves over ripples. *J. Waterw. Port Coastal Ocean Eng.* 112, 309–319.
- Davies, A.G., Heathershaw, A.D., 1984. Surface-wave propagation over sinusoidally varying topography. *J. Fluid Mech.* 144, 419–443.
- Guazzelli, E., Rey, V., Belzons, M., 1992. Higher-order Bragg reflection of gravity surface waves by periodic beds. *J. Fluid Mech.* 245, 301–317.
- Hara, T., Mei, C.C., 1987. Bragg scattering of surface waves by periodic bars: theory and experiment. *J. Fluid Mech.* 178, 221–241.
- Kirby, J.T., 1984. A note on linear surface wave-current interaction over slowly varying topography. *J. Geophys. Res.* 89 (C1), 745–747.
- Kirby, J.T., 1986. A general wave equation for waves over rippled beds. *J. Fluid Mech.* 162, 171–186.
- Kirby, J.T., Anton, J.P., 1990. Bragg reflection of waves by artificial bars. In: *Proc. 22nd Coastal Eng. Conf., New York*, Vol. 1, pp. 757–768.
- Kirby, J.T., Lee, C., Rasmussen, C., 1992. Time-dependent solutions of the mild-slope wave equation. In: *Proc. 23rd Coastal Eng. Conf., Venice*, Vol. 1, pp. 391–404.
- Kubo, Y., Kotake, Y., Isobe, M., Watanabe, A., 1992. Time-dependent mild slope equation for random waves. In: *Proc. 23rd Coastal Eng. Conf., Venice*, Vol. 1, pp. 419–431.
- Larsen, J., Dancy, H., 1983. Open boundaries in short wave simulations: A new approach. *Coastal Eng.* 7, 285–297.

- Lee, C., Suh, K.D. 1997. Internal generation of waves for time-dependent mild-slope equations. Coastal Eng. (submitted).
- Luke, J.C., 1967. A variational principle for a fluid with a free surface. *J. Fluid Mech.* 27, 395–397.
- Madsen, P.A., Larsen, J., 1987. An efficient finite-difference approach to the mild-slope equation. Coastal Eng. 11, 329–351.
- Mansard, E.P.D., Funke, E.R., 1980. The measurement of incident and reflected spectra using a least squares method. In: Proc. 17th Coastal Eng. Conf., Sydney, Vol. 1, pp. 154–172.
- Massel, S.R., 1993. Extended refraction–diffraction equation for surface waves. Coastal Eng. 19, 97–126.
- Massel, S.R., 1994. Measurement and modelling of waves incident on steep islands and shoals. In: Proc. Int. Symp. Waves, Physical and Numerical Modelling, Vancouver, Vol. 2, pp. 982–991.
- Mei, C.C., 1985. Resonant reflection of surface water waves by periodic sandbars. *J. Fluid Mech.* 152, 315–335.
- Miles, J.W., 1981. Oblique surface-wave diffraction by a cylindrical obstacle. *Dyn. Atmos. Oceans* 6, 121–123.
- Nadaoka, K., Beji, S., Nakagawa, Y., 1994. A fully-dispersive nonlinear wave model and its numerical solutions. In: Proc. 24th Coastal Eng. Conf., Kobe, Vol. 1, pp. 427–441.
- O’Hare, T.J., Davies, A.G., 1992. A new model for surface–wave propagation over undulating topography. Coastal Eng. 18, 251–266.
- O’Hare, T.J., Davies, A.G., 1993. A comparison of two models for surface–wave propagation over rapidly varying topography. *Appl. Ocean Res.* 15, 1–11.
- Otnes, R.K., Enochson, L., 1978. *Applied Time Series Analysis, Vol. 1, Basic Techniques*. John Wiley & Sons, New York.
- Park, W.S., Lee, D.S., Oh, Y.M., Jeong, W.M., 1991. Infinite elements for analysis of diffraction and radiation problems in the vertical plane. *J. Korean Soc. Coastal Ocean Engrs.* 3 (4), 235–243, (in Korean, with English abstract).
- Porter, D., Staziker, D.J., 1995. Extensions of the mild-slope equation. *J. Fluid Mech.* 300, 367–382.
- Radder, A.C., 1979. On the parabolic equation method for water–wave propagation. *J. Fluid Mech.* 95, 159–176.
- Radder, A.C., Dingemans, M.W., 1985. Canonical equations for almost periodic, weakly nonlinear gravity waves. *Wave Motion* 7, 473–485.
- Smith, R., Sprinks, T., 1975. Scattering of surface waves by a conical island. *J. Fluid Mech.* 72, 373–384.
- Suh, K.D., Park, W.S., 1995. Wave reflection from perforated-wall caisson breakwaters. Coastal Eng. 26, 177–193.
- Takano, K., 1960. Effects d’un obstacle parallélépipédique sur la propagation de la houle. *Houille Blanche* 15, 247–267.